Revista Brasileira de Cartografia
ISSN 1808-0936 | https://doi.org/10.14393/revbrascartogr
Sociedade Brasileira de Cartografia, Geodésia, Fotogrametria e Sensoriamento Remoto

# Bathymetric DEM derived from Lyzenga's algorithm (multispectral Bathymetry) using Landsat 8 images: a case study of Fort Lauderdale coast

## *MDE batimétrico derivado do algoritmo de Lyzenga (batimetria multiespectral) utilizando imagens Landsat 8: um estudo de caso para a costa de Fort Lauderdale*

César Francisco de Paula [1], Luís Antônio de Lima [2], Jorge Pimentel Cintra [3], Henrique Candido de Oliveira [4] and Diógenes Cortijo Costa [5]

1 Escola Politécnica da Universidade de São Paulo, São Paulo, Brasil. cesardepaula@usp.br.
ORCID: https://orcid.org/0000-0002-6522-8853
2 Universidade de Campinas, Campinas, Brasil. luis@fototerra.com.br.
ORCID: https://orcid.org/0000-0002-5303-5026
3 Escola Politécnica da Universidade de São Paulo, São Paulo, Brasil. jpcintra@usp.br.
ORCID: https://orcid.org/0000-0002-1369-6110
4 The Pennsylvania State University, Wilkes-Barre, USA, hmo5157@psu.edu.
ORCID: https://orcid.org/0000-0002-2783-4668
5 Universidade de Campinas, Campinas, Brasil. dcortijo@unicamp.br.
ORCID: https://orcid.org/0000-0003-0084-6252

Recebido: 03.2023 | Aceito: 07.2023

**Abstract:** Optical bathymetry can be applied to multispectral images of coastal regions with low spectral and spatial resolutions, and the results obtained are satisfactory in waters up to 15 m. However, the limitations and effectiveness may vary as they are related to physical factors such as water turbidity, specular reflection, and the presence of clouds and shadows during imagery acquisition. Some of these factors also affect the surveys conducted using green Light Detection and Ranging (LiDAR) technology. This study aimed to show that topographic representation by multispectral images is directly related to the physical factors of the water body and the atmospheric conditions during the image acquisition process, good atmospheric conditions and shallow water can generate accurate topographic representation. The experiments carried out in this study using optical bathymetry showed that Landsat 8 satellite images could be used in multispectral bathymetry with a linear regression model by using depth samples obtained from shallow water. Images taken at three different time points were used, with a certain time interval between the data collection performed via the Green LiDAR technology. The depths estimated by this model showed some differences that were possibly caused by water turbidity and temporally-occurring activities. Despite such constraints, the depths obtained by the linear regression model showed a good adaptation to the model derived from the Green LiDAR for depths up to 22 m, with an average error of -0.271 m and a root mean square error of 0.936 m.
**Keywords:** Multispectral Bathymetry, Linear Regression, Green LiDAR, Depth Estimation, Topography.

**Resumo:** A batimetria ótica pode ser aplicada com imagens multiespectrais com baixa resolução espectral e espacial, tomadas em regiões costeiras, obtendo resultados satisfatórios em águas com profundidade de até 15 m. No entanto, as limitações e eficácia da técnica podem variar, pois estão relacionadas a fatores físicos como turbidez da água, reflexão especular e presença de nuvens e sombras durante o imageamento. Este estudo tem como objetivo mostrar que a representação topográfica gerada por imagens multiespectrais está diretamente relacionada a fatores físicos do corpo d'água e condições atmosféricas inerentes durante o processo de imageamento. Boas condições atmosféricas e águas rasas sem muita turbidez podem gerar uma representação topográfica precisa. Os experimentos conduzidos neste estudo utilizando a batimetria ótica mostraram que as imagens do satélite Landsat 8 podem ser empregadas em batimetria multiespectral com um modelo de regressão linear treinado a partir de amostras de profundidade coletadas em águas rasas. Foram utilizadas imagens tomadas em três momentos diferentes, com um certo intervalo de tempo entre as coletas realizadas com o Green LiDAR. As profundidades estimadas por este modelo apresentaram algumas diferenças que foram desencadeadas pela turbidez da água e dinâmicas temporais. Apesar destas restrições, as profundidades estimadas pelo modelo de regressão linear mostraram uma boa adaptação ao modelo derivado do Green LiDAR para profundidades de até 22 m, com erro médio de -0,271 m e rms de 0,936 m.
**Palavras-chave:** Batimetria Mulstiespectral, Regressão Linear, Green LiDAR, Estimativa de Profundidade, Topografia.

# 1 INTRODUCTION

Knowing the submerged topography in coastal regions may be of economic, social, and ecological relevance due to its vulnerability to human intervention. It is also a key element development of hydrodynamic models (IRISH; WHITE, 1998; SUTHERLAND et al., 2004), fishing (NISHIDA et al., 2001), mineral exploration (BASU; MALHOTA, 2002), geomorphology (FINKL; BENEDET; ANDREWS, 2005), studies on coastal processes such as erosion, hydrology, sediment deposition (PRANDLE, 2006; HIGGINS; JAFFE; FULLER, 2007) and coral and reef monitoring (GEYMAN; MALLOF, 2019). Therefore, sustainable management is necessary for preserving these regions (mainly the natural resources and ecosystems), while providing opportunities for the economic development of local communities (COSTANZA; FARLEY, 2007; SÁNCHEZ-CARNERO et al., 2012).

Despite quality topographic mappings of the terrestrial portions of the coastal regions being commonly available in the planialtimetric form (typically represented by contour lines or digital elevation models - DEM), data depicting marine regions are still rare. This lack of data is due to the complexity involved in data collection (PICKRILL; TODD, 2003).

Although conventional bathymetry techniques using sound navigation and ranging (SONAR) and Green Light Detection and Ranging (LiDAR) are more accurate and capable of generating good results at submerged areas with greater depths, multispectral images can be a quick and inexpensive alternative to obtain bathymetric models for shallow water. Multispectral bathymetry techniques provide temporal analysis of submerged topography using cataloged images (ROSSI; MAMMI; PELLICCIA, 2019). Additionally, image-based bathymetry techniques may yield good results in shallow waters, especially in intertidal regions (e.g., <5 m), where sonar data collection becomes problematic due to sensor limitations and vessel approach (KIBELE; SHEARS, 2016). One of the main problems with using sonar in shallow waters is echo spreading and reverberation, which generates noise that directly interferes with the representation of the topography and altimetric accuracy (ELLIS, 1994; ABRAHAM; WILLET, 2002).

As shown in this paper, multispectral bathymetry has advantages in shallow water because of its cost-effectiveness, speed in determining the model, accuracy in topographic representation, and higher efficiency at greater depths (provided the water turbidity conditions are good).

This study aimed to evaluate the multispectral bathymetry technique (log-transformation), according to the algorithm proposed by Lyzenga, Malinas and Tanis (2006), for a coastal region located in the city of Fort Lauderdale (Florida, USA). We used Landsat 8 satellite multispectral images from three time points spaced throughout the Green LiDAR survey. The technique's efficiency was verified through images collected under various turbidity conditions at various time intervals and compared with the Green Lidar acquisition. It was also possible to evaluate the variation in the submerged topography and the effectiveness of the topographic representation through models derived from multispectral bathymetry in a time series.

This paper is structured as follows: Section 2 summarizes the SONAR and LiDAR technologies that have been used in bathymetry, and Section 3 presents related works highlighting the methodology used and the results obtained. Section 4 presents the technology that deals with the theoretical seafloor depth. Section 5 presents the study area and the dataset used. Section 6 presents the description of the employed methodology, including data pre-treatment and the obtained result; i.e., the depth estimation by the linear regression method in three datasets corresponding to each of the three time points. The results and conclusions are discussed in Sections 7 and 8, respectively.

# 2 TECHNOLOGIES USED IN BATHYMETRY

## 2.1 SONAR

The acquisition of topographic seafloor information has historically been made with conventional bathymetry techniques that use measurements made by sound sensors (SONAR) attached to boats (GEYMAN; MALOOF, 2019).

Acoustic waves have physical characteristics that differ from other waves, such as light and radio

waves. Acoustic waves are greatly influenced by the medium in which they propagate, and the capacity to generate electric signals is the basic characteristic of every sonar. Such signals are converted into acoustic energy through a transducer that emits a pulse of acoustic energy at a particular frequency. The conversion of acoustic energy into electrical energy occurs through a receiving transducer that separates these echoes from seafloor sound. Additionally, all sonars can accurately associate time, particularly transmission-related time, with the returning echoes. The details of the emission transmitter, receiving transducer, echo processing, and returning echo interpretation distinguish the two types of sonar, single- and multi-beam (HUFF; LLOYYD; NOLL, 2007).

Single-beam sonars typically have one or two transducers designed to transmit and receive acoustic energy at a given frequency. The vertical orientation of the beams determines the interaction between the transmission of acoustic waves and the nearest seafloor (vertically), minimizing the energy of the returning echo. The received echoes are processed to determine the arrival time of the first echo and the time measured by the single beam, which is associated with the shortest distance from the vessel to a point at the bottom of the submerged vessel. The nadir position (depth directly below the survey vessel) depends on vessel stability, main transducer features, and bottom configuration, which may not be the nadir position. In shallow waters, position inaccuracy may be minor. However, due to its dimensions, the sign footprint includes a different depth region around the nadir position at greater depths (HUFF; LLOYYD; NOLL, 2007).

In the case of multi-beam sonars, the depths are not determined only in relation to the nadir position, which implies that they are recorded considering a pre-established angular range. The multi-beam has an exclusive transducer for emitting and receiving echoes for nonvertical angles. All multi-beam sonars measure the travel time between the echo probe transducer and topographic seafloor using an acoustic pulse. One of the main differences between multi-beam and other types of sonar is how the sonar processes and interprets the echo waveforms that are received after pulse transmission (HEALD; PACE, 1996).

A conventional multi-beam sonar measures the acoustic travel time of the echo to the seabed as a function of the pulse position angle with respect to the nadir using trigonometric functions. The travel time results are converted into a set of points with vertical and horizontal coordinates determined in relation to the position of the multibeam transducer. As the geometry of the measurement is nonvertical, it is essential for sensors such as the Global Navigation Satellite System (GNSS) receiver/antenna and Inertial Navigation Systems (INS) to be used in the survey platform together with the sonar for positioning and direct data georeferencing, which requires time synchronization between system components (HUFF; LLOYYD; NOLL, 2007).

A conventional multi-beam sonar has a single linear transmission transducer oriented along the survey line. Its width and length are such that the entire depth measurement range can be identified by the same acoustic pulse. The main lobe of the transmission transducer was narrow in the direction of the track of the vessel along the surface (horizontal plane) and wide in the nadir direction. The receiving transducer, which can be a linear line or circular arc, is an oriented transverse strip with several beams, each with its own main lobe tract, and is relatively wide along the strip (horizontal plane) and narrow towards the cross (vertical plane) (HUFF; LLOYYD; NOLL, 2007).

## 2.2 LiDAR

Another technique for collecting data from the topographic seafloor involves using laser sensors integrated with other elements assembled on an aerial platform. This set of integrated sensors is known as the LiDAR system and has been widely used in three-dimensional mapping over extensive areas of the Earth's surface and submerged regions (rivers, dams and oceans).

The LiDAR system can be divided into four basic units: measurement, scanner (laser pulse), control, and processing. Light beams (lasers) are generated internally by electronic components and photodiodes, which are integral parts of the scanner. The light beams are directed towards a set of rotating mirrors, which through a set of fiber-optic arrays, direct them to the Earth's surface in the form of laser pulses. The transmission of these pulses has limited coverage (range) along a flight line established according to the field of view (FOV) configured a priori in the control unit.

Once the trajectory of the laser pulse (emission and reflection) is developed, it returns to the scanning unit through a set of mirrors and optical fiber matrices and is directed to the measurement unit, whose function is to register the instant when the laser pulse returns to the sensor. The operation of the scanner is registered and controlled at the processing unit, as well as the monitoring and recording of the information measured by the GNSS receiver and INS sensor, both of which are parts of the LiDAR system (WEHR; LOHR, 1999).

The basic function of a laser is to estimate the distance between the sensor and an object, and the accuracy of this measurement is directly related to the precision over time. In the case of lasers integrated into the LiDAR systems, the accuracy of the Time-of-Flight (ToF) is measured by a very short but intense pulse, which travels from the sensor to the object, reflecting in the opposite path and returning to the sensor. Thus, the laser measures the precise time interval between the pulse emitted by the sensor and its return after reflection from an object.

Airborne laser bathymetry (ALB), also known as airborne laser hydrography (ALH), Green LiDAR, or LiDAR bathymetric, is the LiDAR system used for bathymetry. It consists of a green laser (wavelength ~ 532 nm), used for mapping submerged regions, integrated with an infrared laser (wavelength ~ 1064 nm), the objective of which is to collect information on terrestrial portions and the surface of the water body, both working together to produce the data of vast maritime and coastal regions accurately and rapidly (ZHAO et al. 2017a).

This system has been used for bathymetry since 1980 and can collect information with high productivity under adverse weather conditions without interference from sun-glint, even when operating in shallow waters, and provide an accurate topography representation due to its dense cloud of points (GORDON, 1980; GUENTHER, 1985; GUENTHER; CUNNINGHAM; LAROCQUE, 2000; GAO, 2009; ZHAO et al., 2017a; ZHAO et al., 2017b).

## 3 MULTISPECTRAL BATHYMETRY - RELATED WORK

There are studies describing experiments that use the multispectral bathymetric technique to estimate the depth and represent the topographic seafloor. These studies reported experiments on images taken by different sensors, at different resolutions, and under different environmental conditions.

One of the problems encountered during image acquisition with optical remote sensing in water bodies is specular reflection (sun-glint), which directly affects depth estimation in multispectral bathymetry. The authors of a previous study, Lyzenga, Malinas and Tanis (2006) applied sun-glint removal techniques to the multispectral images collected by the IKONOS satellite before estimating the depths by training the linear regression model. The tests were performed using images taken at different periods in certain areas in the Caribbean Sea with depths below 15 m. Removing pixels contaminated by sun-glint has proven to be an effective technique, and multispectral bathymetry showed a root mean square error (RMSE) lower than 2.3 m compared to LiDAR data, which is taken as the standard for comparison.

In the work described by Ellis (1994), the author shows, based on works Lyzenga (1981) and Lyzenga (1985), that the application of KNN (K-Nearest Neighbors) regression yields a more accurate result for the estimation of depths when compared with the linear regression model used by Lyzenga. Both techniques for depth estimation were applied to images taken by the World View (WV) satellite 2 and 3, with spatial resolutions of 0.46 m and 0.31 m, respectively, in the panchromatic band, for an extensive area of the northeast coast of New Zealand, whose maximum depth recorded by a multibeam sonar was less than 23 m. The bathymetric models developed for this study area derived from the WV3 image showed an RMSE of 0.79 m when using the KNN regression and 2.22 m when using the linear regression model proposed by Lyzenga. For the WV2 image, the calculated RMSE was 1.54 m when using the KNN regression and 2.22 m when using the linear regression.

According to the author, the most degraded results using linear regression are due to the method being based on an almost unique dispersion approximation (QSSA) of the radiative transfer equation (RTE) and predicated on the transformation of the observed radiation, which generates a negative linear relationship with depth in all types of bottoms.

The work presented by Pacheco at al. (2014), similar to that proposed in this study, shows the

effectiveness of multispectral bathymetry using the Lyzenga method when applied to Landsat 8 images taken of two regions of the coast of Portugal. The author highlights the potential of using images available for free to monitor and manage coastal morphological evolution. The results obtained showed high accuracy in the bathymetric model developed for depths of up to 8 m and reinforced that the efficiency of this method is directly related to the optical imaging system.

Applying the Stumpf model (log-ratio model) in multispectral bathymetry combined with Landsat 8 images also effectively estimated shallow water depths. In the experiment carried out in Jagalingam, Akshaya and Hegde (2015), the authors applied the Stumpf model to a Landsat 8 image of an area on the southwest coast of India. The multispectral bathymetry model, together with the multibeam derived model, has proven to adapt satisfactorily at a maximum depth of 20 m with a correlation ($R^2$) of 0.878.

As presented in the related work summarized below, multispectral bathymetry can generate an accurate topographic representation for shallow waters using images provided by Landsat 8.

# 4 THEORETICAL BACKGROUND

## 4.1 Green LiDAR Data Collection and Processing

Green LiDAR is a technology that can be used to map the submerged topography in water bodies, provided the wavelength emitted by this sensor propagates in the water, covering the path up to the topographic bottom and reflecting the emitted laser pulse (MANDLBURGUER et al., 2015). Besides propagating in water, the green light is also reflected on the terrestrial surface, mainly in vegetation coverings, thus registering information on objects located outside the water body.

In the topographic model provided by this system, it is necessary to know the limit of the water surface a priori, and hence, topobathimetric LiDAR systems are used, which have green and infrared lasers integrated into their set (ZHAO et al., 2017). Hence, in the topobathimetric LiDAR system, the infrared laser used to delimit the water surface as part of the emitted pulses undergo specular reflection, and the green laser is used to map the submerged topographic seafloor. Figure 1 shows a graphical scheme of the LiDAR profile of a water body obtained using a topobathimetric system.

Figure 1 - Graphical layout of LiDAR profiling in water bodies using the topobathimetric system.

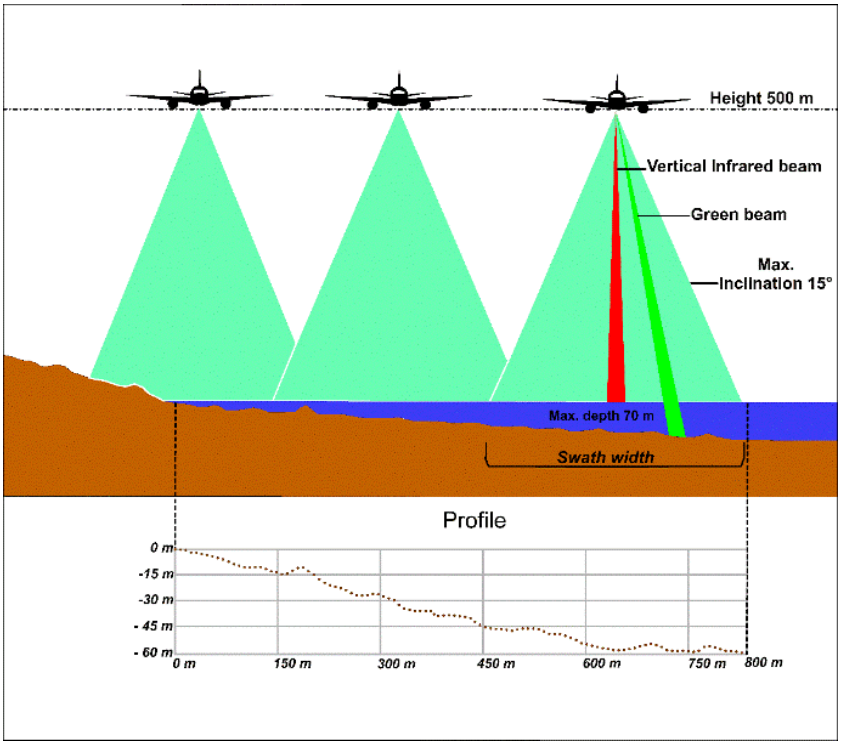


Source: Authors (2023).

In this example, the topobathimetric LiDAR system was installed 500 m above the water surface in an aircraft. The infrared laser pulse is emitted in the nadir direction, undergoing specular reflection on the water surface; i.e., the angle of reflection is equal to the emission angle, which causes the return of the emitted laser pulse to the sensor to record the signal.

For the green laser, the pulse emitted depends on a previously set FOV value, and it will travel its path through the atmosphere and will continue to propagate in the water where, after a certain depth (70 m maximum), it will find the topographic seafloor and then reflect back to the system on the aircraft. In the workflow for processing topobathimetric data, it is necessary to classify the point cloud from the two laser sensors and separate the points representing the water body surface from those representing the submerged topography. This classification is performed using algorithms similar to those used to identify ground points in profiles that use only topographic LiDAR (AXELSSON, 1999; MA, 2005).

In the Green LiDAR data processing phase, it is necessary to correct and/or minimize the effects caused by issues such as reflection, refraction of the green pulse on the water surface, scattering and turbidity (which directly influence the signal propagation), and attenuation of the pulse return if it results in a low signal-to-noise ratio (SNR) (PAN et al., 2015).

Among the effects of the green laser pulse, light refraction directly interferes with the three-dimensional topographic model representation, as its effect provides an apparent displacement. Therefore, when the laser pulse passes from air to water (or water to air), a decrease in the propagation of light in water or a change in the angle of incidence is noticed because of different light refraction indices. Based on Snell's law, the refraction of light in water can be corrected by considering the horizontal surface of the water body to be completely flat (WESTFELD et al., 2016).

Additionally, it should not be ignored that the surface of a water body contains waves that cause other deviations and allow for errors in the depth measurement. Hence, special attention must be given to deeper regions. Figure 2 shows the effect of light refraction on a green laser pulse, with a notable three-dimensional displacement in determining the representation of the topographic seafloor. A DEM can be generated by interpolating the dense point cloud, processing, and georeferencing to obtain a three-dimensional model of the submerged topography.

Figure 2 - Schematic illustrating the effect of light refraction on water bodies in modeling the submerged topography.

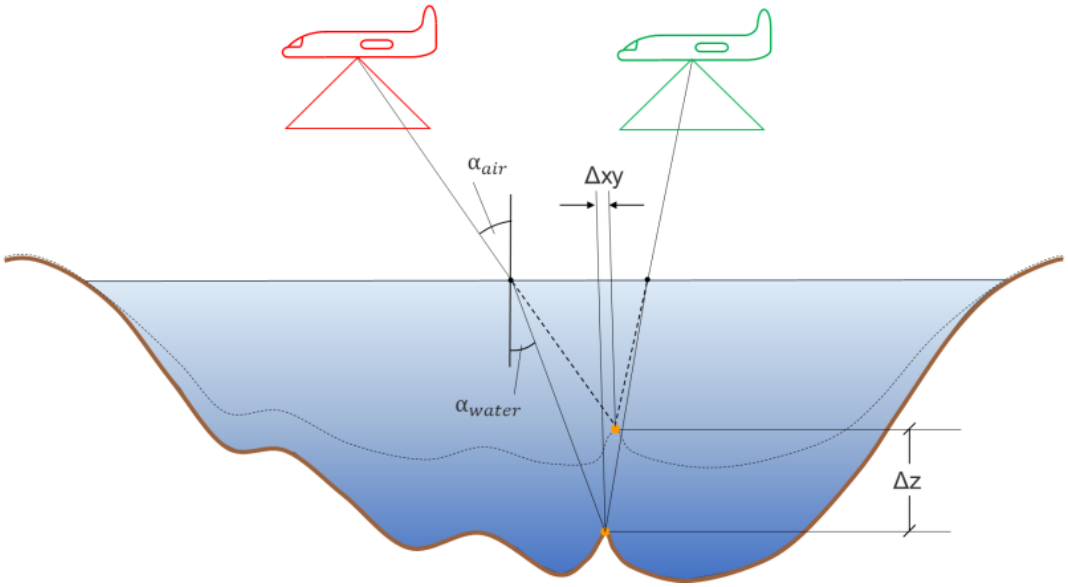


Source: Mandlburger et al. (2015).

## 4.2 Multispectral Bathymetry

Some studies used satellite images with high spectral and spatial resolution, which show a good representation of submerged topography (DENG; JI; ZHANG, 1979; MAHMUD; HASAN; ESTATE, 2017). However, the feasibility of using low spectral and spatial resolution satellite images (average spatial resolution

of approximately 15 m or larger) should be considered to develop bathymetric information at a low cost for coastal regions that lack bathymetry information.

Multispectral bathymetry techniques are based on the attenuation of electromagnetic radiation at different wavelengths when it penetrates a water body. In the model used for optical bathymetry (Eq. (1)), all parameters except depth are dependent on the wavelength. It is assumed that all water properties are kept homogeneous in different directions, and although not true, it is considered a starting point (PHILPOT, 1989).

$$L_d = L_b \exp(-g.z) + L_w \quad (1)$$

where: $L_d$ is radiance observed by the sensor, $L_b$ radiance of the band sensitive to the topographic seafloor, $g$ radiance attenuation coefficient in water, $z$ water column depth and the $L_w$ is radiance observed in deep-water area.

The development of Eq. (1) has led to efficient methods for modeling multispectral bathymetry. Two of these are most commonly used: the model proposed by Lyzenga (1981) (Log-Linear Model) and the model proposed by Stumpf et al., (2003) (Log-Ratio Model).

In the method proposed by Lyzenga (1981), the radiation in a water body can be represented by a linear function of the reflectance of the topographic seafloor, and the depth is represented by an exponential function. The independent albedo method (reflection coefficient) was used to create a bathymetric model from a multispectral image, considering that the attenuation of light in a water body occurs according to exponential variation. Thus, a linear mathematical model was obtained, which relates the radiance number in "N" spectral bands with the water depth (Eq. (2)).

$$\hat{Z} = h_0 + \sum_{j=1}^{N} h_j \ln(Lb_j - \overline{Lb_j^{\propto}}) \quad (2)$$

where: $\hat{Z}$ is calculated depth value, $h_0$ and $h_j$ are coefficients determined by linear regression for each spectral band used in the model, $Lb_j$ the radiance values in spectral band j and the $\overline{Lb_j^{\propto}}$ is average radiance value in the band j for a region of great depth in the water body.

In the method proposed by Stumpf, a logarithmic transformation is used to linearize the relationship between the radiance of the spectral band and depth. In this model, a pair of bands is used to decrease the number of parameters and estimate the depths. As the bands are evenly distributed, errors caused by the variation of radiation in the atmosphere, water column, and bottom of the water body are minimized (PUSHPARAJ; HEGDE, 2017). Eq. (3) presents the Stumpf model for estimating shallow water depths.

$$\hat{Z} = h_1 \frac{\ln(n(Lb_i))}{\ln(n(Lb_j))} - h_0 \quad (3)$$

where: $\hat{Z}$ is calculated depth value, $h_0$ and $h_1$ are coefficients determined by linear regression, $n$ is constant value chosen to maintain a positive ratio for any reflectance value, $Lb_i$ is radiance observed in spectral band *I* and the $Lb_j$ radiance observed in spectral band *j*.

## 5 STUDY AREA AND DATASET

### 5.1 Multispectral Images

The experiments were conducted in a region on the coast of Fort Lauderdale (Florida, USA), in an area of approximately 1.9 km², located at 25.956088° N and 80.114445° W (Figure 3).

The Landsat 8 images used in this experiment were taken at three time points (Table 1), spaced between the time of acquisition of the Green LiDAR data (two before and one after 2015). We chose three distinct time points for analyzing the possible effects of water elements, such as turbidity and sun-glint, and those occurring

at the seafloor due to siltation, sediment deposition, and algae, coral, and reef growth.

Table 1–- Time and conditions in which the multispectral images were taken.

| Imagem Date | Time (UTC) | Solar Azimuth (deg. - °) | Sun Elevation (deg. - °) |
|---|---|---|---|
| 18/01/2014 | 15:51:11 | 149.788° | 37.486° |
| 23/03/2014 | 15:50:23 | 132.599° | 55.786° |
| 19/01/2018 | 15:50:06 | 150.515° | 36.729° |

Source: Authors (2023).

Regarding the dates of the chosen images, we first conducted a search in the catalogue to determine which ones were cloud-free and close to the date when the collection with Green LiDAR was performed, assuming that this would result in minimal variation in the representation of the seafloor topography when comparing the results.

The selection of images with close dates (18/01/2014 and 23/03/2014) aimed to evaluate the variation in the topographic representation generated by the multispectral bathymetry technique over a short time interval (due to occurring dynamics), as well as to attempt to correlate the influence of the physical conditions of the water in the application of the technique.

The image taken on a more distant date (19/01/2018) from LiDAR survey was intended to assess how much the seafloor topography had changed after a significant time interval.

Figure 3–- Spatial map of the study area chosen to perform the multispectral bathymetry.

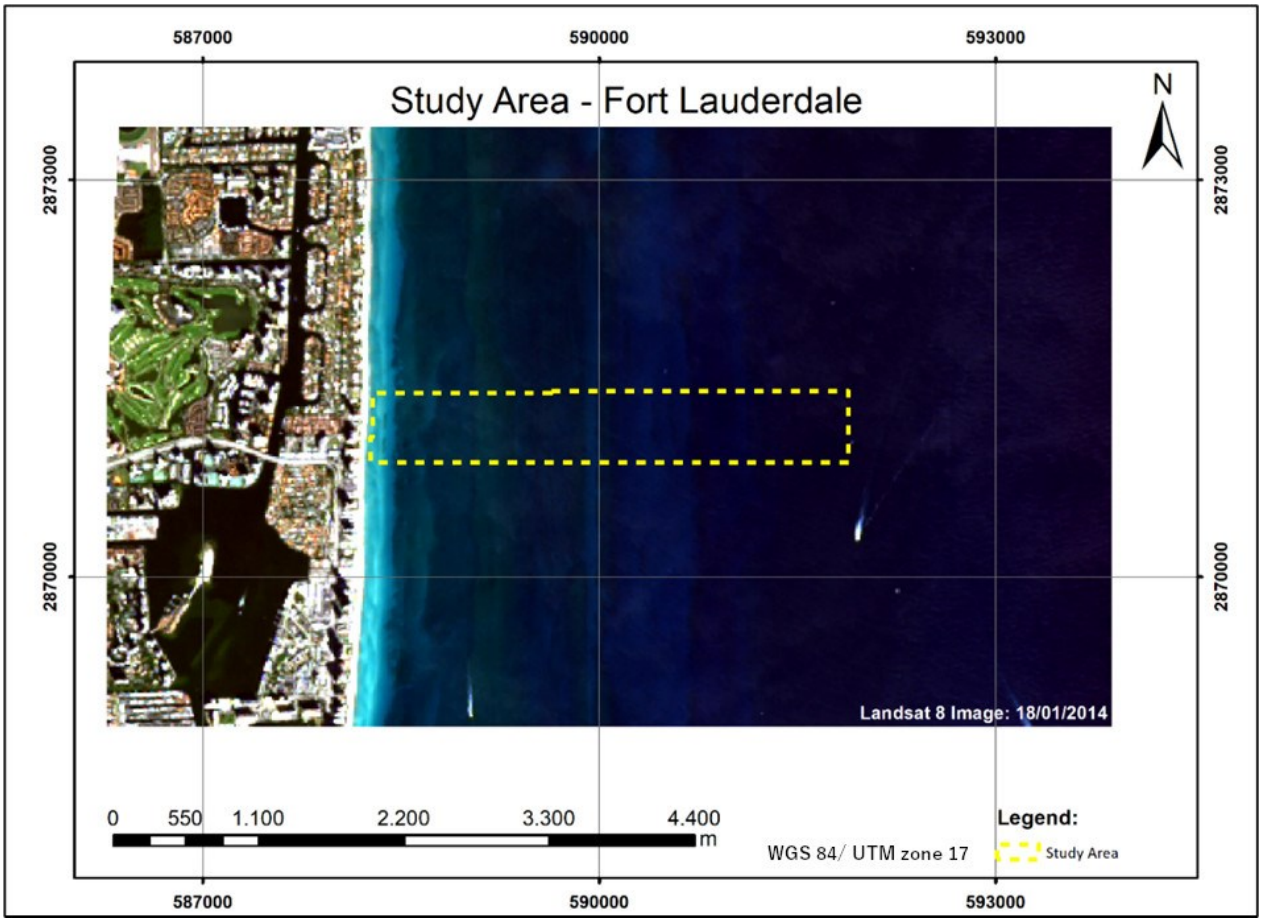


Source: Authors (2023).

It is important to state that this work applies the technique of multispectral bathymetry in shallow waters. The definition of the depth inherent to the classification presents variation depending on type of study, however, in this work, we will consider that shallow water is those whose depth does not exceed 30 meters.

## 5.2 Green LiDAR

The Green LiDAR data, provided by Optech, were collected in a campaign carried out by the company on June 15, 2015. The data collection for Fort Lauderdale was carried out using the Optech CZMIL sensor. After the direct georeferencing of the collected data, a dense cloud of points with an average density of 3.24 pts/m² was obtained, enabling a detailed representation of the topographic seafloor of the area of interest. According to Optech, the altimetric values obtained by post-processing the Green LiDAR dataset were corrected for the interferences of the tide that were registered when the flight was performed. The topographic model of the seafloor obtained using Green LiDAR was used as a standard for comparison with other models derived from multispectral bathymetry.

# 6 METHODOLOGY FOR DEPTH ESTIMATION AND RESULTS

In this section, the steps for obtaining depth models derived from multispectral bathymetry based on the method proposed by Lyzenga are described (workflow presented in Figure 4).

Figure 4 – Schematic showcasing the workflow for the experiment using Lyzenga's approach.

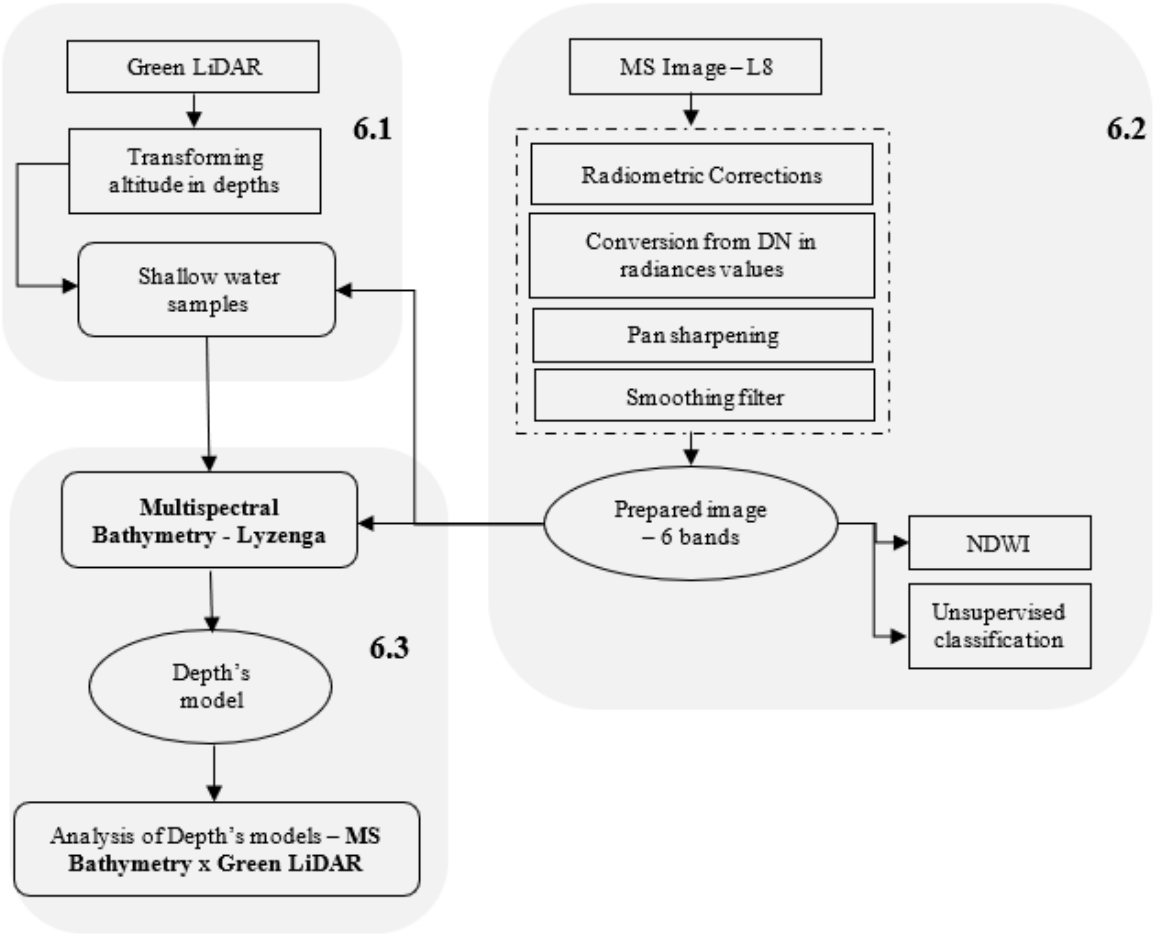


Source: Authors (2023).

## 6.1 LiDAR Point Cloud Treatment

The LiDAR point cloud, which generated a regular square mesh with a spacing of 1 m, was interpolated to obtain the DEM.

The normalization of altitudes was performed considering the points of LiDAR cloud taken with the topographic LiDAR (collected at the same time with Green LiDAR) that were registered on the water surface. Since all the points of the cloud (water surface and submerged topography) had elevations, subtracting them allowed obtaining a depth model (Figure 5).

Figure 5 – Color gradient scheme depicting the depth model derived from the Green LiDAR data.

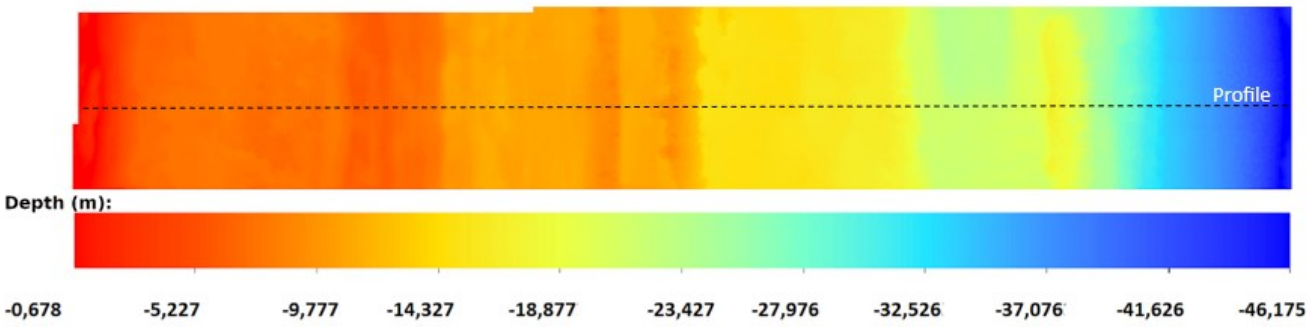


Source: Authors (2023).

## 6.2 Treatment of Multispectral Images

Each Landsat 8 image (three time points) received the following treatments: radiometric corrections to reduce the effects of the atmosphere, conversion of digital numbers to radiance values, and pan-sharpening to obtain all the stacked bands in a single raster file and resampled to 15 m spatial resolution. This procedure resulted in a 6-spectral-band image (blue, green, red, near-infrared, SWIR-1, and SWIR-2). Satellite images commonly present fragmentation problems, and hence, a smoothing filter was applied to homogenize pixels and eliminate water noises, which tend to interfere in the image classification process, mainly in the water regions (KOURGLI, 2013).

Following the methodological workflow (Figure 4), the normalized difference water index (NDWI—Eq. (4)) was calculated for each of the three image sets so that the water mass could be delineated from the dry coastland (McFEETERS, 1996).

$$\boldsymbol{NDWI} = \frac{\boldsymbol{X}_{Green} - \boldsymbol{X}_{Near-Infrared}}{\boldsymbol{X}_{Green} - \boldsymbol{X}_{Near-Infrared}} \quad (4)$$

The delimitation of the water portion along the area of interest followed the limits within the DEM and was obtained by LiDAR and NDWI profiling. Figure 6 depicts some important cutouts of the multispectral images, showing the water bodies used in the three experiments, corresponding to the same study area at three different time points.

Figure 6 - Multispectral images of the water mass at the three time points selected for this study.

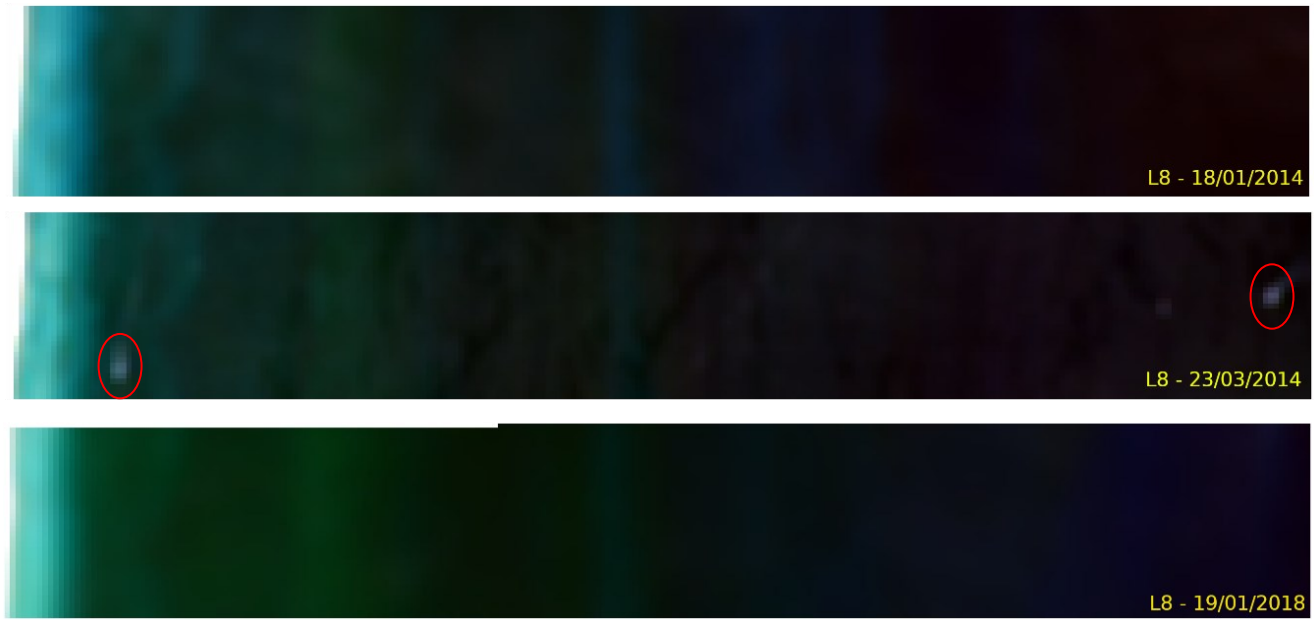


Source: Authors (2023).

In Figure 6, for image taken on 23/03/2014, there are two red ellipses highlighting regions containing brighter pixels. These regions refer to boats that were moving in the area at the time when the imaging by Landsat 8 was conducted, as the complete scene shows the trajectory of the boats marked in the image. This observation is relevant to the study because at first time suggests the occurrence of sun-glint effect.

Through multispectral image processing, water areas were selected using an unsupervised classification approach (using k-means algorithm implemented on Orfeo plugin for QGIS software) to distinguish two regions: shallow water and deep water. The darker images suggest greater turbidity in the water, which can be seen in the image taken on 23/03/2014.

## 6.3 Depth Estimation Using Linear Regression

Before applying the linear regression method, a logarithmic transformation was performed for each spectral band in the Landsat 8 images. As shown in Eq. (5), the transformation is applied to the pixel values of each band, subtracted from the mean radiance value calculated for a sample extracted from a deep-water region. In the bands transformed a priori, it was possible to observe No Data values in the pixels for which subtraction between the radiances returned negative values. The average radiances calculated for the deep-water samples were multiplied by ten standard deviations to avoid pixels with No Data values. Thus, the logarithmic function was applied to only positive values. This approach was also used by Kibele e Shears (2016) to avoid the occurrence of No Data after log transformation.

$$X_j = \ln(Lb_i - L_{si}) \tag{5}$$

where: $Lb_i$ is radiance values in the band $i$ and $L_{si}$ is mean radiance value calculated in the band i for a sample extracted from a deep-water region.

With the log-transformed bands and depth samples for a shallow water area, linear regression model training (Eq. (2)) was performed, and the coefficients $h_0$, $h_1$, and $h_2$ for each time point were obtained. A random coastal area depicting 107 sample points was chosen, wherein, after non-supervised image classification, we identified the area as a shallow water area. For training the regression model, the information of bands R, G, and B and the depth model was transferred as attributes to the sampling points.

The depth values of the sample points used in the training of the linear regression model were extracted from the DEM derived from the Green LiDAR, thus making the vertical data compatible among the generated models. The correlation between the spectral bands in this study was calculated by pairs; however, it is possible to combine "N" spectral bands simultaneously in multispectral bathymetry, mainly when using hyperspectral images. Table 2 shows the correlation between the pairs of bands in the training of the model and their associated coefficients.

Table 2 - Correlation between the bands and linear regression coefficients calculated when training the model for the three time points.

| | 18/01/2014 | | | 23/03/2014 | | | 19/01/2018 | | |
|---|---|---|---|---|---|---|---|---|---|
| | B/G | B/R | G/R | B/G | B/R | G/R | B/G | B/R | G/R |
| **$R^2$** | **0.972** | 0.958 | 0.963 | **0.969** | 0.961 | 0.967 | **0.955** | 0.935 | 0.947 |
| **$h_0$** | 5.390 | 5.325 | 6.148 | 6.533 | 8.228 | 7.909 | 10.714 | 7.497 | 9.565 |
| **$h_1$** | -6.418 | 1.362 | 2.356 | -6.855 | 2.529 | 3.284 | -5.208 | 2.474 | 4.592 |
| **$h_2$** | 10.361 | 0.979 | 0.665 | 11.769 | 0.967 | 0.666 | 12.175 | 0.552 | 0.201 |

Source: Authors (2023).

As expected, the greatest correlation ($R^2$) for all the three time points was found for the blue and green band pairs. The other pairs (Blue/Red and Green/Red) closely correlated with the first pair (Blue/Green), probably because no great variations in the objects were identified in the image that contained only the water body. The low correlation values when having the combined red band can be explained by its attenuation in the water, decreasing with increasing depth and not with reflectance values due to the effect caused by very

shallow waters where the values can be higher than those of other bands.

In Table 2, the indices $h_0$, $h_1$, and $h_2$ correspond to the coefficients obtained by the linear combination, considering the numbers of sample point depths and the blue and green log-transformed bands, respectively.

Equations 6 – 8, derived from the numbers in Table 4, present the models used in the depth estimates for the three time points using the blue and green log-transformed bands, respectively.

$$\boldsymbol{Z_{18/01/2014}} = 5.390693 - 6.418182.\boldsymbol{X_{Blue}} + 10.361218.\boldsymbol{X_{Green}} \quad (6)$$

$$\boldsymbol{Z_{23/03/2014}} = 6.533670 - 6.855303.\boldsymbol{X_{Blue}} + 11.769556.\boldsymbol{X_{Green}} \quad (7)$$

$$\boldsymbol{Z_{19/01/2018}} = 10.714696 - 5.208486.\boldsymbol{X_{Blue}} + 12.175262.\boldsymbol{X_{Green}} \quad (8)$$

where: $\boldsymbol{Z}$ is estimated depth in each model at different time points, $\boldsymbol{X_{Blue}}$ is blue band log-transformed and $\boldsymbol{X_{Green}}$ is green band log-transformed.

Figure 7 shows the depth models (meters) developed using the multispectral bathymetric technique, separated by time: (A) – 18/01/2014, (B) – 23/03/2014 and (C) – 19/01/2018.

Figure 8 shows a longitudinal profile drawn on the depth models developed by the Green LiDAR (represented in green), as well as by multispectral bathymetry applied for the three time points (red, blue, and magenta). The position of the longitudinal profile made is shown by dashed black line shown in Figure 5.

Figure 7 - Color gradient scheme depicting depth model derived from multispectral bathymetry from the L8 image taken on 18/01/2014 - (A), 23/03/2014 - (B) and.19/01/2018 – (C), respectively.

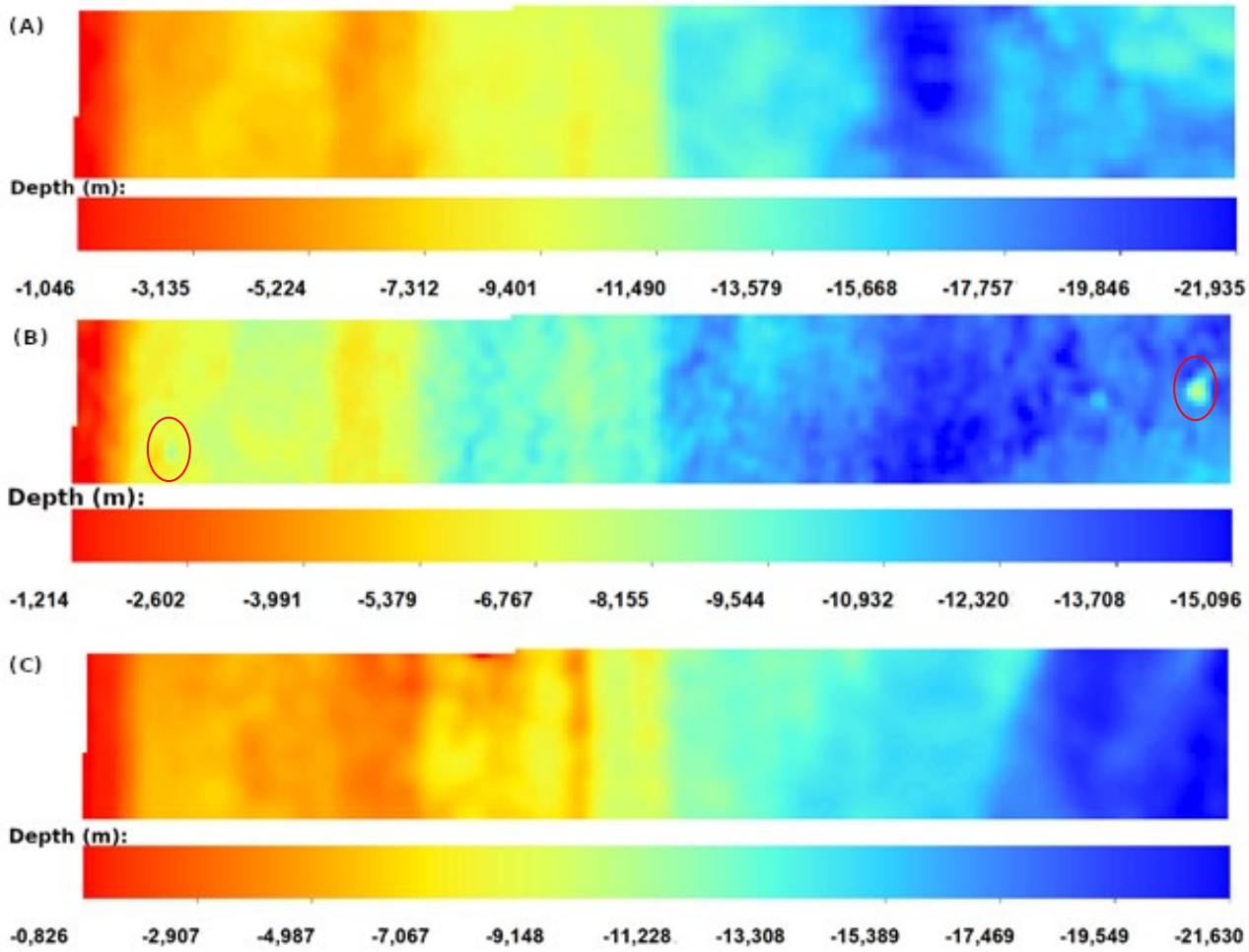


Source: Authors (2023).

In Figure 7 (B), it is possible to observe two highlighted regions containing noise in the representation of the bathymetric model derived from multispectral bathymetry, which coincide with the highlighted regions in Figure 6, for brighter pixels regions.

Figure 8 – Line graph of the profile from the Green LiDAR model and the models developed for the three time points.

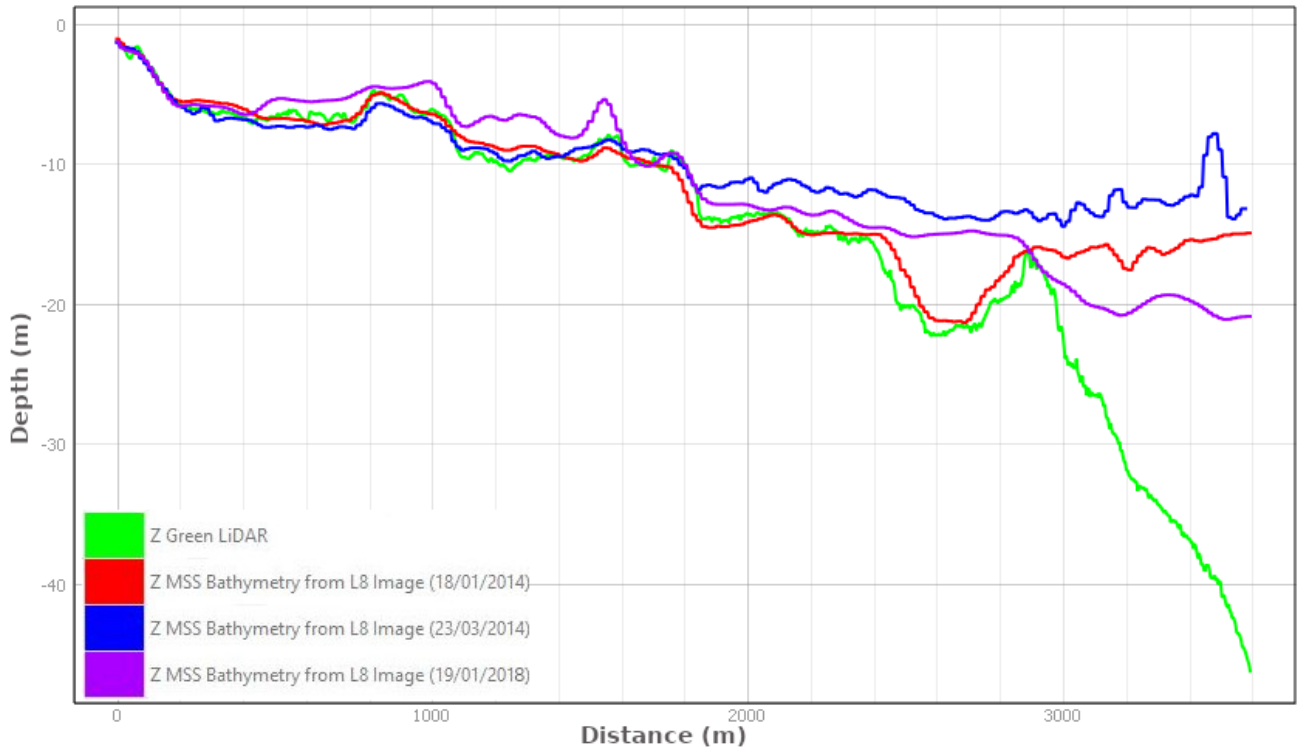


Source: Authors (2023).

## 7 DISCUSSION

Figure 8 shows that for the shallower part (minimum depth: up to ~ 8 m), all models fall close to each other; however, in the deepest regions, there is a big difference in the maximum depth of the models derived from the multispectral bathymetry when compared with that of the model generated by Green LiDAR. The differences found at greater depths are directly related to the water quality due to scattering and attenuation of the radiant energy caused by suspended particles and dissolved materials such as tannin or yellow substances.

The profiles presented show a good adaptation of the submerged topography of the Green LiDAR model to the models generated by multispectral bathymetry using imagens taken on 18/01/2014 and 23/03/2014, for regions with depths of up to 10 m, approximately. The most accurate representation is shown on profile represented in red, corresponding to the model generated from the image taken on 18/01/2014, which presents a time interval of 18 months in relation to the LiDAR data acquisition.

For depth models derived from images taken in 2014, little variation in the representation of the topography of their models was expected, as the images had an interval of only two months between their acquisition.

As shown in Figure 8 (profile represented in blue), the bathymetric model developed from the image taken on 23/03/2014 generated a different result from the model generated by the image taken on 18/01/2014, where topographic depression is not represented in the profiles derived from LiDAR and the image taken on 18/01/2014. This difference or deficiency in the topographic representation seen in the profile represented in blue may be due to phenomena such as sun-glint and turbidity of the water body present during imaging and not due to variations in the submerged topography. The higher turbidity in this image was evidenced through histogram analysis, which revealed a significant shift towards lower intensity values and a reduction in the presence of higher intensity values.

Other images from the Landsat 8 sensor were available closer to the LiDAR capture dates; however, these were captured under cloudy weather conditions, which negatively affected the processing of the model. The representation of the topography generated by this image (23/03/2014) proved to be coherent for maximum depths up to 10 m. High turbidity in water also could explains part the degradation in the topographic representation in the bathymetric model, as shown in Figure 6, which affects deeper areas where poor light incidence is a common event.

As mentioned earlier, Figure 6 shows two regions with brighter pixels that correspond to moving boats in the area of interest when the Landsat 8 image was taken. This occurrence introduced noise in the same regions of the derived model from multispectral bathymetry (Figure 7), which resembles the behavior observed when applying the technique to images with evident specular reflection on the water surface, affecting the topographic representation in these regions.

Several tests were conducted on this image in an attempt to minimize the effect of these brighter pixels on the bathymetric model. In the image, these pixels were considered as sun-glint and the approach described in Lyzenga, Malinas and Tanis (2006) was applied. Using the new image, the multispectral bathymetry technique described in this paper was applied, resulting in another bathymetric model that differed from the model derived from the image before sun-glint removal a was also distinct from the model derived from Green LiDAR.

The Green LiDAR model showed the divergence of adaptation to an area based on the profiles obtained and presented in Figure 8 for the following dates: 23/03/2014 and 19/01/2018. On profile represented on blue color, the separation with the LiDAR profile is more evident at a depth of 10 m, whereas on profile represented on magenta color, the separation occurs at three depth intervals: ~ 8–10 m, ~ 12–17 m, and above 19 m.

The difference in adaptation between the profiles can be explained by the possible turbidity of the water, as the image taken on 23/03/2014 is darker than the others (Figure 6). By analyzing the results presented on profile represented by magenta color, we can hypothesize that this difference may have occurred because of the variation in topography in these areas due to the seafloor dynamics (sediment deposit or algae growth) over time and reinforced by the temporal difference (42 months) in the data collected by Green LiDAR. The hypothesis that water turbidity may influence the generation of the model cannot be ruled out, although its interference was slightly lower for the results shown because there is an adaptation between the profiles at a depth of ~ 20 m.

The models generated by multispectral bathymetry and Green LiDAR were also compared through residual calculation (Figure 9), depth correlation, and precision, as graphically shown in Figure 10. The analysis considered a depth increase interval of 2 m. Most residues in Figure 9 are at a 5 m level. Shallower areas depict lower numbers (coastal), while deeper waters depict more residues, particularly where bathymetry models reveal high image degradation. The evident positive values in Figure 9 occur because in some regions within the study area, the models derived from multispectral bathymetry are above the model derived from Green LiDAR.

The graphs in Figure 10 show the maximum depths at which multispectral bathymetry is efficient. The scatter plot built from the bathymetric model developed by the image taken on 18/01/2014 (Figure 10 - A) shows that up to a depth of 22 m, there is a high correlation of the model ($R^2 = 0.975$) with the depths derived from Green LiDAR and an average error of -0.271 m. In the bathymetric model derived from the image taken on 23/03/2014, the greatest correlation ($R^2 = 0.945$) was found for depths of up to 8 m at that particular time point, with an average error of 0.530 m. For the most distant time point (19/01/2018), the best correlation was found for a maximum depth of 8 m ($R^2 = 0.786$) and an average error of -0.760 m.

The linear regressions were evaluated using the hypothesis test (t-test), where the coefficients were assessed together with their standard errors and testes considering a 95% confidence interval ($t = \pm 1.984$). The values obtained in the test indicated that all coefficients of the three linear regression model are statistically significant.

 DOI: http://dx.doi.org/10.14393/rbcv75n0a-68742

Figure 9 - Color gradient scheme depicting residues calculated between the depth models from Green LiDAR and the model derived from the image taken on 18/01/2014 (A), 23/03/2014 (B), and 19/01/2018 (C).

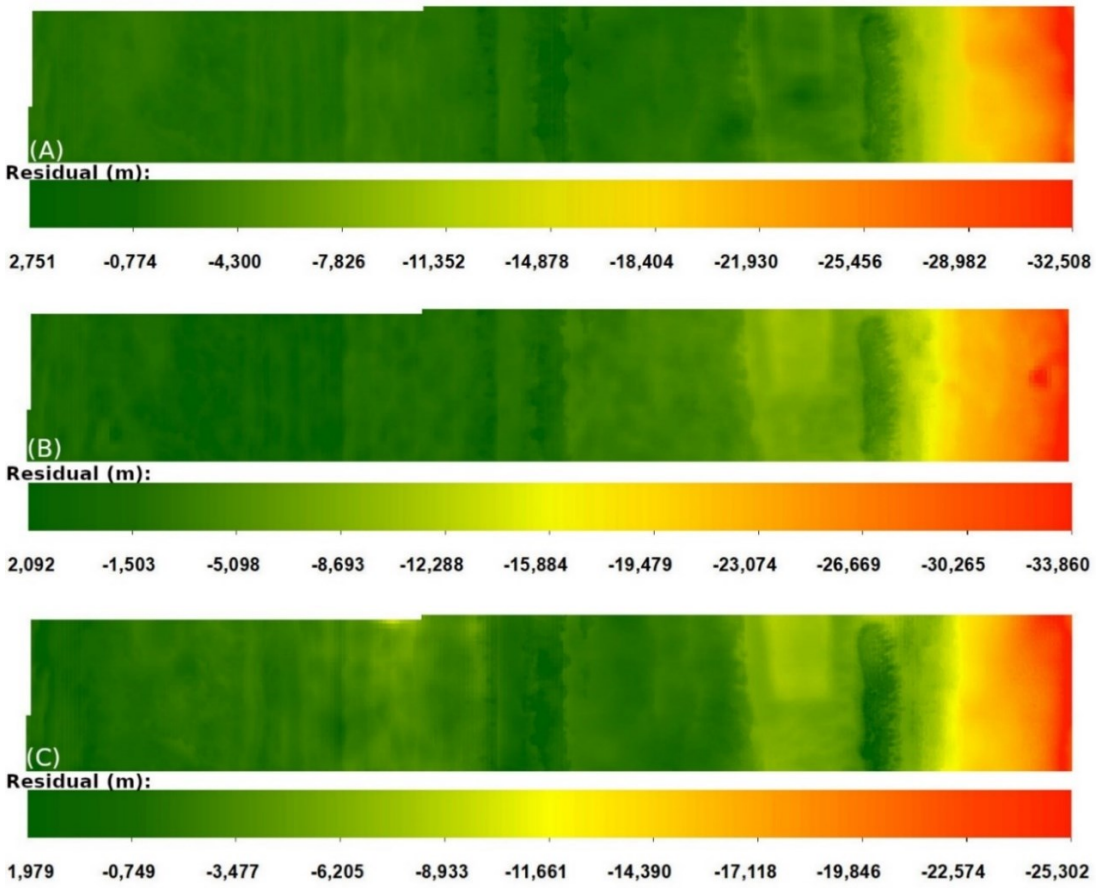


Source: Authors (2023).

Figure 10 - Scatter plot between true and estimated ground depths: (A) time point: 18/01/2014, (B) time point: 23/03/2014, and (C) time point: 19/01/2018.

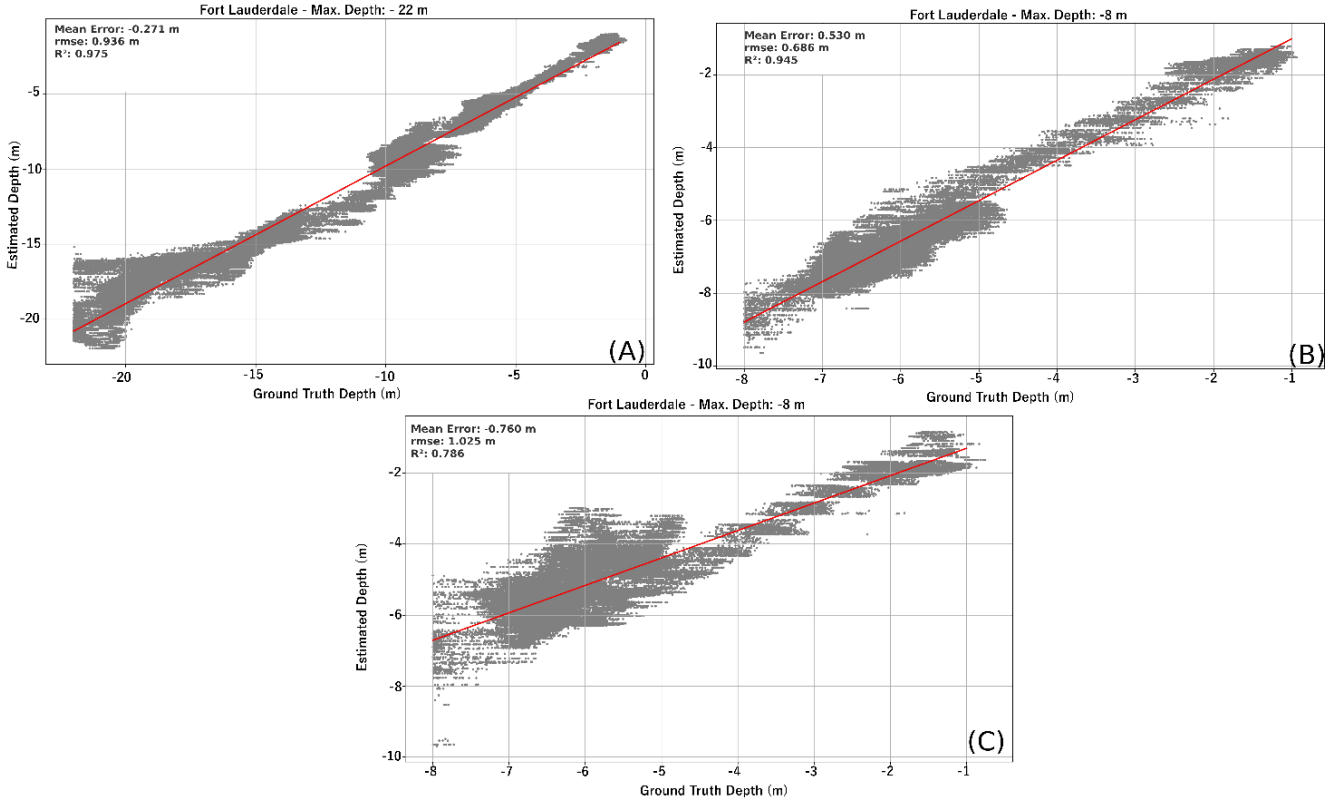


Source: Authors (2023).

# 8 CONCLUSIONS

Prior to knowing the importance of learning about submerged topography and its variations over time, multispectral bathymetry models have provided good estimations of depth using Landsat 8 satellite images. It has proven to be an excellent alternative for constructing coastal and inland water models at low cost for areas devoid of topographic representation and for shallow waters. The quality of the obtained results may have been influenced by the environmental conditions of the water body during imaging and may also be linked to variations in submerged topography resulting from long-term action of marine currents. Given the temporal difference between the analyzed models (MS Bathymetry x Green LiDAR), it is plausible to suggest that some of the observed discrepancies between them are associated with topographic changes, such as sedimentation or sediment deposition.

The effectiveness of the multispectral bathymetric models, as found in the model from the 23/03/2014 image, might be affected by water turbidity and its influence at a maximum depth of 8 m. The topography and depths derived from this image are expected to be close to those of the model built from the image taken in January of the same year. The specular reflection may also have contributed to the degradation of the image, as Figure 6 shows some white pixels in two areas (punctual and highlighted in the image) that occurred because of the movement of boats during the imaging process, thereby producing an effect similar to that of sun-glint (Figure 7).

Time interval is also a variable that must be considered when developing bathymetric models using the multispectral bathymetry technique derived. In our experiments, we used images taken on different dates and with a temporal distance from the date when the Green LiDAR dataset was acquired.

This temporal disparity might have been a contributing factor to the observed variations in depth between the generated models. Some of these variations could potentially be correlated with submerged dynamics, such as the action of marine currents, which may have occurred more or less intensively in deep waters, resulting in sedimentation or particle deposition (e.g., sand) on the topographic seabed.

To assert the topographic variation found in the model generated with an image acquired 42 months apart from the Green LiDAR data acquisition, a comprehensive study investigating the impact of maritime dynamics would be necessary. Hence, we emphasize the significance of conducting studies that elucidate the nature and intensity of submerged dynamics at the time of acquiring the multispectral images in temporal bathymetric analyses. Based on the behavior of these dynamics, it is conceivable that a portion of the differences observed in the models can be attributed to these phenomena.

The removal of the sun-glint effect in the images using Lyzenga's approach is effective in removing and/or minimizing the effects generated in the images, which directly affects the bathymetric representation when derived from optical bathymetric techniques (LYZENGA; MALINAS AND TANIS, 2006). A disadvantage of this technique is that the proposed model changes the original number of radiances in areas free from contamination by sun-glint. This reduces the efficiency of multispectral bathymetry when developing the model. The sun-glint removal test performed using the image obtained on 23/03/2014 was found to be effective. However, the derived bathymetric model was satisfactory only for depths up to 6 m.

Generally, multispectral bathymetry is shown to estimate shallow water depths effectively; however, it is important to emphasize that the greatest challenge of this technique is studying the influence of certain phenomena on water bodies, which is a limiting factor for different data sets.

The approach introduced by Lyzenga in his multispectral bathymetry algorithm, applied in this study, demonstrated that depth models in shallow waters can be obtained using freely available archived images. However, the quality of representativeness of the generated models may be compromised by the influence of certain variables present in the water body during acquisition or image capture, which are not addressed by the proposed algorithm.

Although the multispectral bathymetry models may not precisely represent the topographic seafloor, they can still be valuable for preliminary maritime studies. Additionally, when analyzed in conjunction with other variables, these models have the potential to generate hypotheses that deserve further investigation.

As presented in this paper, multispectral bathymetry can be performed through a linear regression model as well as through an exponential logarithmic function. The experiments conducted in this paper used

multispectral bathymetry with linear regression model. However, we consider it important to conduct studies using both approaches. Thus way, mor conclusions can be draw and new hypotheses can be tested.

We would also like to suggest further research on the application of multimedia bathymetry for obtaining depth models in shallow waters. The models generated using different techniques (Green LiDAR, Multispectral Bathymetry and Multimedia Bathymetry) can be compared and their representative qualities of the topography can be better evaluated. It also suggested to use tests performed with the residuals found in order to confirm their normality. Among the suggested tests are the Shapiro-Wilk and Kolmogorov-Smirnov.

## Acknowledgements

Thanks to the companies Teledyne Optech and Engesat for yielding the input data used in the experiment. It has been an important support to this work. The company Fototerra for the incentive and interest in the results of this research.

This paper is part of the study of the Doctoral research of the first author, César Francisco de Paula, which is was financed in part by the CAPES – process number 88881.187052/2018-01.

## Author's Contribution

**C.F.P.:** Conceptualization, Data Curation, Formal Analysis, Acquisition of Financing, Research, Methodology, Supervision, Writing - initial draft, Writing - revision and editing. **L.A.L:** Conceptualization, Data Curation, Formal Analysis, Acquisition of Financing, Validation, Writing - initial draft. **J.P.C.:** Conceptualization, Formal Analysis, Acquisition of Financing, Methodology, Validation, Writing - initial draft. **H.C.O.:** Conceptualization, Formal Analysis, Research, Methodology, Visualization, Writing - revision and editing. **D.C.C.:** Conceptualization, Formal Analysis, Research, Supervision, Writing - revision and editing.

## Interest Conflicts

The authors declare that they have no known competing financial interests or personal relationships that could have appeared to influence the work reported in this paper.

## References

ABRAHAM, D. A.; WILLETT, P. K. Active sonar detection in shallow water using the page test. **IEEE Journal of Oceanic Engineering**, v. 27, n. 1, p. 35–46, 2002. DOI. 10.1109/48.989883.

AXELSSON, P. Processing of laser scanner data - Algorithms and applications. **ISPRS Journal of Photogrammetry and Remote Sensing**, v. 54, n. 2–3, p. 138–147, 1999. DOI. 10.1016/S0924-2716(99)00011-8.

BASU, A.; MALHOTRA, S. Error detection of bathymetry data by visualization using GIS. **ICES Journal of Marine Science**, v. 59, n. 1, p. 226–234, 2002. DOI. 10.1006/2001.1147.

COSTANZA, R.; FARLEY, J. Ecological economics of coastal disasters: Introduction to the special issue. **Ecological Economics**, v. 63, n. 2–3, p. 249–253, 2007. DOI. :10.1016/2007.03.002.

DENG, Z.; JI, M.; ZHANG, Z. Mapping Bathymetry from Multi-Source Remote Sensing Images: A Case Study in the Beilun Estuary, GUANGXI , CHINA. **The International Archives of the Photogrammetry, Remote Sensing and Spatial Information Sciences**, Beijing, Vol. XXXVII. Part B8, p. 1321–1326, 2008. ISSN 1682-1750.

ELLIS, D. D. A shallow-water normal-mode reverberation model. **The Journal of the Acoustical Society of America,** v. 97, n. May, p. 2804–2814, 1994. DOI. 10.1121/1.411910.

FINKL, C. W.; BENEDET, L.; ANDREWS, J. L. Interpretation of Seabed Geomorphology Based on Spatial Analysis of High-Density Airborne Laser Bathymetry. **Journal of Coastal Research**, v. 213, n. 213, p. 501–514, 2005. DOI. 10.2112/05-756A.1.

GAO, J. Bathymetric mapping by means of remote sensing: Methods, accuracy and limitations. **Progress in Physical Geography**, v. 33, n. 1, p. 103–116, 2009. DOI. 10.1177/0309133309105657.

GEYMAN, E. C.; MALOOF, A. C. A. Simple Method for Extracting Water Depth From Multispectral Satellite Imagery in Regions of Variable Bottom Type. **Earth and Space Science**, v. 6, n. 3, p. 527–537, 2019. DOI. 10.1029/2018EA000539.

GORDON, H. R. Ocean remote sensing using laser. **US National Oceanic & Atmospheric Administration, Seattle, Washington, Pacific Marine Environmental Laboratory Technical Memorandum**, , n. NOAA-TM-ERL-PMEL-18, 1980.

GUENTHER, G. C. **Airborne Laser Hydrography: System Design and Performance Factors**. 1 Ed. ed. Springfield, 1985.

GUENTHER, G. C.; CUNNINGHAM, A. G.; LAROCQUE, P. E. Meeting the Accuracy Challenge in Airborne Lidar Bathymetry. **EARSeL eProceedings**, v. 1, n. 1, p. 1–27, 2000. DOI. 10.1590/s1982-21702018000300025.

HEALD, G**.** J.; PACE, N. G. Implications of a bi-static treatment for the second echo from a normal incident sonar. **Proceedings of 3rd European Conference on Underwater Acoustics**, p. 649–554, 1996.

HIGGINS, S. A.; JAFFE, B. E.; FULLER, C. C. Reconstructing sediment age profiles from historical bathymetry changes in San Pablo Bay, California. **Estuarine, Coastal and Shelf Science**, v. 73, n. 1–2, p. 165–174, 2007. DOI. 10.1016/2006.12.018.

HUFF, LLOYD C., NOLL, G. T. Sonar. **Digital Elevation Model Technologies and Applications: The DEM Users Manual**. Second Edi ed., p.321–350, 2007. Maryland.

IRISH, J. L.; WHITE, T. E. Coastal engineering applications of high-resolution lidar bathymetry. **Coastal Engineering**, v. 35, n. 1–2, p. 47–71, 1998. DOI.10.1016/S0378-3839(98)00022-2.

JAGALINGAM, P.; AKSHAYA, B. J.; HEGDE, A. V. Bathymetry Mapping Using Landsat 8 Satellite Imagery. **Procedia Engineering**, v. 116, n. Apac, p. 560–566, 2015. Elsevier B.V. DOI: 10.1016/2015.08.326.

KIBELE, J.; SHEARS, N. T. Nonparametric Empirical Depth Regression for Bathymetric Mapping in Coastal Waters. **IEEE Journal of Selected Topics in Applied Earth Observations and Remote Sensing**, p. 1–9, 2016. DOI.10.1109/2016.2598152.

KOURGLI, A.; OUKIL, Y. Very High Resolution Satellite Images Filtering. **2013 Eighth International Conference on Broadband, Wireless Computing, Communication and Applications**, Compiegne – France, 465-470, 2013/28-30. DOI. 10.1109/BWCCA.2013.81.

LYZENGA, D. R. Remote sensing of bottom reflectance and water attenuation parameters in shallow water using aircraft and landsat data. **International Journal of Remote Sensing**, v. 2, n. 1, p. 71–82, 1981. DOI.10.1080/01431168108948342.

LYZENGA, D. R. Shallow-water bathymetry using combined lidar and passive multispectral scanner data. **International Journal of Remote Sensing**, v. 6, n. 1, p. 115–125, 1985. DOI. 10.1080/01431168508948428.

LYZENGA, D. R.; MALINAS, N. P.; TANIS, F. J. Multispectral bathymetry using a simple physically based algorithm. **IEEE Transactions on Geoscience and Remote Sensing**, v. 44, n. 8, p. 2251–2259, 2006. DOI. 10.1109/TGRS.2006.872909.

MA, R. DEM Generation and Building Detection from Lidar Data. **American Society for Photogrammetry and Remote Sensing**, v. 71, n. 7, p. 847–854, 2005. DOI. 0099-1112/05/7107–0847.

MAHMUD, M. R.; HASAN, R. C.; ESTATE, R. SATELLITE-DERIVED BATHYMETRY: ACCURACY ASSESSMENT ON DEPTHS DERIVATION ALGORTITHM FOR SHALLOW WATER AREA. **ISPRS**, v. XLII, n. October, p. 159–164, 2017. DOI. 10.5194/isprs-archives-XLII-4-W5-159-2017.

MANDLBURGER, G.; HAUER, C.; WIESER, M.; PFEIFER, N. Topo-Bathymetric LiDAR for Monitoring River Morphodynamics and Instream Habitats—A Case Study at the Pielach River. **Remote Sensing Journal**, n.4 May 2014, p. 6160–6195, 2015. DOI. 10.3390/rs70506160.

MCFEETERS, S. K. The use of the Normalized Difference Water Index (NDWI) in the delineation of open water features. **International Journal of Remote Sensing**, v. 17, n. 7, p. 1425–1432, 1996. DOI.10.1080/01431169608948714.

NISHIDA, T.; MOHRI, M.; ITOH, K.; NAKAGOME, J. Study of bathymetry effects on the nominal hooking rates of yellowfin tuna (Thunnus albacares) and bigeye tuna (Thunnus obesus) exploited by the Japanese. **IOTC Proceedings**, v. 4, n. 4, p. 191–206, 2001. Disponível em: http://wwe.iotc.org/sites/default/files/documents/proceedings/2001/wpm/IOTC-2001-WPM-02.pdf.

NATIONAL OCEANIC AND ATMOSPHERIC ADMINISTRATION (NOOA). **U. S. Departament of Commerce**. São Paulo, 2020. Disponível em: https://tidesandcurrents.noaa.gov/stationhome.html?id=8722956. Acesso em: 30 abr. 2020.

PACHECO, A.; HORTA, J.; LOUREIRO, C.; FERREIRA, Ó. Remote Sensing of Environment Retrieval of nearshore bathymetry from Landsat 8 images: A tool for coastal monitoring in shallow waters. **Remote Sensing of Environment,** 2014. Elsevier Inc. DOI: 10.1016/j.rse.2014.12.004.

PAN, Z.; GLENNIE, C.; HARTZELL, P.; HARTZEL, P.; DIAZ, J. C. F; LEGLEITER, C.; OVERSTREET, B. Performance assessment of high resolution airborne full waveform LiDAR for shallow river bathymetry. **Remote Sensing**, v. 7, n. 5, p. 5133–5159, 2015. DOI.10.3390/rs70505133.

PHILPOT, W. D. Bathymetric mapping with passive multispectral imagery. **Applied Optics**, v. 28, n. 8, p. 1569, 1989. DOI.10.1364/AO.28.001569.

PICKRILL, R. A.; TODD, B. J. The multiple roles of acoustic mapping in integrated ocean management, Canadian Atlantic continental margin. **Ocean and Coastal Management**, v. 46, n. 6–7, p. 601–614, 2003. DOI. 10.1016/S0964-5691(03)00037-1.

PRANDLE, D. Dynamical controls on estuarine bathymetry: Assessment against UK database. **Estuarine, Coastal and Shelf Science**, v. 68, n. 1, p. 282–288, 2006. DOI.10.1016/j.ecss.2006.02.009.

PUSHPARAJ, J.; HEGDE, A. V. Estimation of bathymetry along the coast of Mangaluru using Landsat-8 imagery. **International Journal of Ocean and Climate Systems**, 2017. DOI.10.1177/17593131166796.

ROSSI, L.; MAMMI, I.; PELLICCIA, F. UAV multispectral images for bathymetry estimation. **IMEKO TC-19 – International Workshop on Metrology for the Sea**, Genoa, p. 119–124, 2019. DOI. 10.21014/actaimeko.v12i3.1684.

SÁNCHEZ-CARNERO, N.; ACEÑA, S.; RODRÍGUEZ-PÉREZ, D.; COUÑAGO, E.; FRAILE, P.; FREIRE, J. Fast and low-cost method for VBES bathymetry generation in coastal areas. **Estuarine, Coastal and Shelf Science**, v. 114, n. December, p. 175–182, 2012. Elsevier Ltd. DOI: 10.1016/j.ecss.2012.08.018.

STUMPF, R. P.; HOLDERIED, K.; SPRING, S.; SINCLAIR, M. Determination of water depth with high-resolution satellite imagery over variable bottom types. **Limnology and Oceanography**, v. 48, p. 547–556, 2003. DOI.10.4319/Io.2003.48.1.

SUTHERLAND, J.; WALSTRA, D. J. R.; CHESHER, T. J.; VAN RIJN, L. C.; SOUTHGATE, H. N. Evaluation of coastal area modelling systems at an estuary mouth. **Coastal Engineering**, v. 51, n. 2, p. 119–142, 2004. DOI.10.1016/2003.12.003.

WEHR, A.; LOHR, U. Airborne laser scanning - An introduction and overview**. ISPRS Journal of Photogrammetry and Remote Sensing**, v. 54, n. 2–3, p. 68–82, 1999. DOI.10.1016/S0924-2716(99)00011-8.

WESTFELD, P.; RICHTER, K.; MAAS, H. G.; WEISS, R. Analysis of the effect ofwave patterns on refraction in airborne lidar bathymetry. **International Archives of the Photogrammetry, Remote Sensing and Spatial Information Sciences - ISPRS Archives**, v. 2016-Janua, n. July, p. 133–139, 2016. DOI.10.5194/133-2016.

ZHAO, J.; ZHAO, X.; ZHANG, H.; ZHOU, F. Shallow water measurements using a single green laser

corrected by building a near water surface penetration model. **Remote Sensing**, v. 9, n. 5, p. 1–18, 2017a. DOI.10.3390/rs9050426.

ZHAO, J.; ZHAO, X.; ZHANG, H.; ZHOU, F. Improved model for depth bias correction in airborne LiDAR bathymetry systems. **Remote Sensing**, v. 9, n. 7, p. 1–16, 2017b. DOI.10.3390/rs9070710.

## Biography of the main author

César Francisco de Paula was born in Itaú de Minas (MG) in 1983. Cartographer Engineer from UNESP (Universidade Estadual Paulista). Master and PhD candidate in Transportation Engineering from EPUSP (Escola Politécnica da Universidade de São Paulo). The thesis presents research related to multimedia and multispectral bathymetry Applied to water reservoir in Brazilian context. Part of doctoral research was developed at the Institute of Photogrammetry at University of Stuttgart, Germany. He currently works as coordinator of Aerophotogrammetry and Remote Sensing at Fototerra Company – Brazil, developing projects of different scales and purposes.